*Short Paper*

# Visual Assessment of Vascular Torsion using Ellipse Fitting

Gabriel Mistelbauer[1] ![ORCID], Martin Zettwitz[1], Rüdiger Schernthaner[2], Dominik Fleischmann[3], Christian Teutsch[4], Bernhard Preim[1]

[1]Dept. of Simulation and Graphics, Otto-von-Guericke University Magdeburg, Germany
[2]Dept. of Biomedical Imaging and Image-Guided Therapy, Medical University of Vienna, Austria
[3]Stanford University School of Medicine, Stanford, CA, USA
[4]Fraunhofer Institute for Factory Operation and Automation, Magdeburg, Germany

## Abstract
*Blood vessels are well explored and researched in medicine and visualization. However, the investigation of vascular torsion has yet been unexplored. In order to understand the development and current state of a single blood vessel or even multiple connected ones, properties of vascular structures have to be analyzed. In this paper we assess the torsion of blood vessels in order to better understand their morphology. The aim of this work is to quantitatively gauge blood vessels by using an automated method that assumes an elliptical blood vessel model. This facilitates using state-of-the-art ellipse fitting algorithms from industrial measuring standards. In order to remove outliers, we propose a self-correcting iterative refitting of ellipses using neighboring information. The torsion information is visually conveyed by connecting the major and minor points of adjacent ellipses. Our final visualization comprises a visual representation of the blood vessel including four bands to outline the torsion.*

## CCS Concepts
*• Computing methodologies → Parametric curve and surface models; Shape analysis;*

## 1. Introduction

Quantitatively analyzing the morphology of blood vessels is important for surgery simulation and planning. Many aspects have been studied well, such as the visualization of vascular structures [WWL*10]. They are commonly represented as a graph with circular cross-sections spread equidistantly across its edges. These vessels can then be visualized as truncated cones [HPSP01] or convolution surfaces [OP04]. However, cross-sections of blood vessels usually do not exhibit a circular shape, but rather an elliptical. During a surgery, when suturing two different blood vessels, an important aspect is their torsion [LLC09]. Brown et al. [BMLS01] propose a simulation of joining two vessels during a microsurgery. As twisting of the joined blood vessels should be avoided, a visualization of a vessel's torsion would increase the confidence of surgeons.

In this paper, we propose a visualization technique that depicts the torsion of blood vessels. This approach requires a segmentation of the desired vessels in order to extract their centerlines. However, this segmentation does not have to be exact, since our technique is robust against inaccuracies. In summary, our contributions are:

- a robust torsion visualization of segmented vascular structures,
- an iterative cross-sectional ellipse fitting approach, and
- a self-corrective elliptical model fitting.

In the remainder of this paper, we discuss related work (see Section 2), followed by our approach (see Section 3). After presenting and discussing results (see Section 4), the paper is concluded with future remarks (see Section 5).

## 2. Related Work

Torsion in blood vessels arises from body movement or surgery [HLJ16, GSF*17], especially the arteries in the neck are vulnerable to strong and abrupt movement [HLJ16] and also curved vessels will exhibit torsion due to the natural minimization of the surface energy. Also reduced axial tension or elongation of arteries leads to torsion, as well as weakened arterial walls due to lack of elastin [Han12]. While minor torsion has no significant effect, higher torsion is distributed to the weakest point of the vessel [TBIC03], since vessels are mechanically unstable under heavy torsion [GSF*17]. This affects high torque, lumen pressure [HLJ16, GSF*17], sheer stress [MY01] and results in buckling, twisting and kinks when torque suddenly drops [HLJ16, GSF*17]. Organ dysfunctions are immediate consequences of these phenomena [GSF*17]. The aortic arch has significant torsion due to its large curvature at the top, where it connects the ascending and descending aorta. The torsion of the aortic arch is related to thoracic aneurysms [MY01]. In contrast to torsion, tortuosity and its effects are widely researched. Since tortuosity arises from torsion and aging, its symptoms are directly linked to torsion [Han12, XYZ13]. Tortuosity is present in almost all parts of the body like large arteries and veins, as well as small arterioles and venules [Han12]. While mild tortuosity is asymptomatic, severe tortuosity yields complications like high load on vessels, sheer stress, curling and curving, twisting, looping and kinking [Han12, FCCH17]. These complications result in energy loss and ineffective blood flow due to the centrifugal effect, which leads to diseases like hypertension or atherosclero-

sis [XYZ13]. Tortuosity is linked to thrombosis [FCCH17], especially in case of coronary arteries [XYZ13], diabetes [FCCH17] and cervical artery dissection that occurs spontaneously or after trauma in relatively young patients (approx. age of 40 years), which leads to ischemic stroke [JKYK*16]. Hence, visualizing torsion or tortuosity might improve disease identification and even prevention.

Representations of vascular structures are generally subdivided into model-based and model-free [PO08]. Former approaches mainly use centerlines and diameters to describe vessels with circle-based cylinders or truncated cones, even though the natural shape is often not circular, but elliptical. Their limitations are poor quality at bifurcations [WWL*10] and the fact that they do not consider cross-sectional shape changes, which makes them unsuitable for surgery simulation [LLC09]. Model-free approaches are based on B-spline surfaces, simplex meshes or MPU implicits [SOB*07]. They describe the shape of a vessel better and model cross-sectional shape changes such as stretching or bending. Their limitations are low accuracy or a high number of polygons [WWL*10] and the difficulty of determining torsion [LLC09]. A basic model-free approach is marching cubes that heavily depends on the chosen iso-value and exhibits artifacts, such as staircases. Wu et al. [WWL*10] describe a scale-adaptive method for modeling the surface of vessels. They use segmented boundary voxels as the basis of an oriented point cloud. A 3D indicator function that is robust against fine noisy perturbations interpolates or approximates the surface points. Afterwards, the interpolated points are adaptively polygonized by adding triangles to the mesh based on curvature and shape of the desired watertight surface. This approach produces less but well-shaped triangles with higher density on detailed areas. Kretschmer et al. [KBT*12] describe another adaptive approach that is based on centerlines and is especially well-defined at bifurcations. Implicit functions describe the cross-sectional shape of vessel segments along their centerlines and they are combined by Boolean operations without intersections. The surface is defined by watertight and scale-adaptive meshes that exhibit high quality with a low number of polygons.

Li et al. [LLC09] describe a hybrid approach to model vessels and visualize their torsion. A 3D mesh and generalized cylinders are used to model deformations, while torsion is modeled physically correct, based on Cosserat rod theory—an approach for modeling elastic tubular structures. The medial axis is computed by fitting a generalized cylinder to the mesh. The mesh vertices correspond to the cylinder and, therefore, to the position on the medial axis and the angle of the cross-section. This approach is able to compute the torsion minimizing configuration by minimizing the torsion energy of vessel joins. However, it cannot compute the torsion of segmented volume data since the torsion must be known in advance. A simplified circular model is described by Mori and Yamaguchi [MY01]. The torsion is computed as a vector product of the tangent (direction of the curve) and the principal normal vector (direction of curvature) along the centerline. There are different metrics of torsion [LLC09, GIK*10]. The Frenet torsion measures the twisting of the space curve about the medial axis, but is ill-posed at inflection points (sign flips). The material torsion measures the rotation of the material line, that is a reference line on the surface computed by rotation minimizing frame around the medial axis. Georgakarakos et al. [GIK*10] project the centerline into a plane and measure its length on $1cm^2$, hence torsion is given in $1/cm^2$.

## 3. Methodology

Since computing and visualizing the torsion of blood vessels requires their centerlines, they have to be segmented first [HPSP01]. As skeletonization is commonly applied to extract the centerlines of segmented blood vessels, noise on the segmentation boundaries impacts the quality of the result. To remedy this issue, holes in the segmentation are filled and the boundary is smoothed prior to the skeletonization. Nevertheless, spurious branches might still remain that have to be detected and removed afterwards [SPSP02]. All these steps are based on case-specific heuristics. If the boundary is smoothed too much, small details are removed. The same holds for spurious branches, which are either defined by their relative length to a main branch or by their absolute length [SPSP02]. There is no single solution for all cases.

We propose an approach without such heuristics. Our algorithm requires segmented blood vessels with their centerlines, but they do not have to be perfectly centered. At equidistant positions along these centerlines, we compute the rotation-minimizing coordinate frame [WJZL08] to extract perpendicular cross-sections. The consistency of the local coordinate frames across branches is ensured by preserving the tangent and one axis to compute the second one. Within these cross-sections, we have the segmentation mask of the current vessel marked as foreground and all other pixels as background. As the centerline is the origin of the extracted slice, the largest connected component around it defines our vessel cross-section, supported by morphological operators. Then, an ellipse is fit to the foregrounds boundary pixels such that outliers are mostly ignored. This procedure is repeated equidistantly along all vessels.

The result of our approach is presented in Figure 1. This visualization reveals the torsion of blood vessels, outlined by the four colored bands that connect the major (green) and minor (yellow) axis points of consecutive fitted ellipses. In this particular case, the abdominal aorta splits in the common iliac arteries, which exhibit a torsion due to their posterior bending. This is clearly depicted in our visualization. The ellipse fitting and its visual mapping are described in the following subsections.
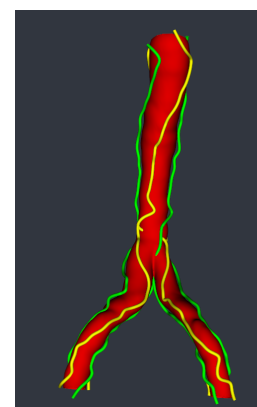


**Figure 1:** *Outcome of our approach. The surface is based on ellipses that have been fit to the input segmentation. The torsion of the aorta and common iliac arteries is depicted by the colored bands, with green connecting the major axis points and yellow the minor ones.*

### 3.1. Iterative Ellipse Fitting

In the literature, there are two categories of least-squares curve fitting, i.e., the algebraic fitting and the geometric fitting. These differ in their respective definition of the error measure that is minimized. A highly representative class of curves is the algebraic curve described by an implicit polynomial equation. Here, an ellipse is described by a general conic as an implicit second order polynomial with the coefficients **b**:

$$F(\mathbf{b}, x) = ax^2 + bxy + cy^2 + dx + ey + f = 0. \quad (1)$$

$F(\mathbf{b}, x)$ is called the algebraic distance, i.e., if $F(\mathbf{b}, x_i) \neq 0$ the point $x_i$ does not lie on the ellipse and there is some error-of-fit. The ellipse fitting can be approached by minimizing the sum of squared algebraic distances of $m$ given points $x$:

$$\min_{\mathbf{b}} \sum_{i=1}^{m} F^2(\mathbf{b}, x_i). \quad (2)$$

Because the algebraic distance $F(\mathbf{b}, x)$ is expressed in linear terms of the algebraic parameters, the algebraic fitting has a computationally efficient closed-form solution [Tau91]. The drawbacks of algebraic fitting are an unclear physical interpretation of the algebraic distance with regard to real applications and a lower accuracy for incomplete and noisy data compared to the geometric fitting. Even if improvements have been made by, e.g., normalization or applying restrictive constraints [HF98, FPF99], the drawbacks remain.

In contrast, the geometric least-squares fitting minimizes the orthogonal distance of the given points to the ellipse, which has a clear physical interpretation, because it is the geometrically shortest distance. The distance of a query point $x_i$ to the ellipse is measured from the closest point $x_i'$, whose normal is directed towards the query point. The geometric least-squares minimization problem is:

$$\min_{\mathbf{b}} \sum_{i=1}^{m} \left\| x_i - x_i' \right\|^2. \quad (3)$$

Geometrically, a 2D ellipse with two radii $a$ and $b$ centered at the position **x** is given by

$$f(a, b, \mathbf{x}) = \frac{x^2}{a^2} + \frac{y^2}{b^2} - 1 = 0, \quad (4)$$

and a fifth parameter, $\varphi$, which is the rotation angle of the longer ellipse axis $a$ with regard to the $x$-axis. The closest point to an ellipse can be computed with a Newton method [Ahn04] as the solution of the linear equation system:

$$\begin{pmatrix} \frac{x}{a^2} & \frac{y}{b^2} \\ \frac{(y_i - y)}{a^2} + \frac{y}{b^2} & \frac{-(x_i - x)}{b^2} - \frac{x}{a^2} \end{pmatrix} \begin{pmatrix} \Delta x \\ \Delta y \end{pmatrix} = - \begin{pmatrix} \frac{x^2}{2a^2} + \frac{y^2}{2b^2} - \frac{1}{2} \\ \frac{(y_i - y)x}{a^2} - \frac{(x_i - x)y}{b^2} \end{pmatrix}. \quad (5)$$

In summary, the geometric fitting needs to approximate the five parameters of the 2D ellipse, which can be done with a Levenberg-Marquardt solver. Within each iteration, the closest point to the ellipse contour needs to be computed, which is an iterative procedure as well. Thus, the geometric ellipse fitting requires a lot of work but provides the benefits of accuracy, numerical robustness and the shortest distance error measure. We have tested both approaches and finally found the geometric approach more reliable, especially for sparse point distributions, noise and some degenerate shapes. A survey on algebraic and geometric ellipse fitting techniques is given by Kanatani et al. [KSK16].

### 3.2. Iterative Outlier Refitting

During this first ellipse fitting iteration, we do not use any prior information, resulting in several potential outlier ellipses as demonstrated in Figure 2, where the abdominal aorta branches to the renal arteries. An ellipse positioned at index $i$ along a vessel centerline is considered an outlier if $|A_i - \overline{A}| > T_A$, or $|\varphi_i - \overline{\varphi}_i| > T_\varphi$, or $ratio(a, b)_i > T_{ratio}$, while $T$ indicates the maximum allowed deviation threshold. Note that $\overline{A}$ is the median ellipse area of the centerline along a branch and $\overline{\varphi}_i$ denotes the median angle over a given neighborhood of $i$. Ellipses marked as outliers are removed and investigated in the next step, leaving disconnections.

In the second iteration the area and ratio outlier ellipses are peeled, i.e., we consecutively delete the outer layers of the input segmentation mask, refit the ellipse and evaluate it until it is below the maximum allowed deviations $T_A$ and $T_{ratio}$. After every peeling step, we refit the ellipse with its new input mask and evaluate the output. This process is done with a diminishing radius of the layers so that outliers further away are deleted first and we converge within the allowed deviation and a percentage-based safety margin ε. We found this step crucial on bifurcations, since the centerline and its tangents will result in strongly intersecting cross-sections with degenerated ellipses, as shown in Figure 4c.

From the third iteration onwards, all ellipses along the centerline of a vessel are refit using its well-shaped neighboring ellipse as prior information. Then, outliers are identified, removed and refit again. For an ellipse $\mathcal{E}_i$ being an outlier and $\mathcal{E}_{i-1}$ or $\mathcal{E}_{i+1}$ as its well-shaped neighbors, $\mathcal{E}_i$ is refit using $\mathcal{E}_{i-1}$ and $\mathcal{E}_{i+1}$ as prior information, respectively. To prevent refit ellipses being angle outliers, we interpolate $\varphi_i$ of the refit ellipses with respect to $\varphi$ of $\mathcal{E}_j$ and $\mathcal{E}_k$, being the surrounding well-shaped start and end points of a disconnection. This step is repeated until all outlier ellipses are refit.

That last iteration handles the ellipses that were yet unable to be fit properly. For this purpose, we simply interpolate all parameters of $\mathcal{E}_i$ between $\mathcal{E}_j$ and $\mathcal{E}_k$ and take the ellipse as it is. These iterations are repeated a user-specified number of times (five iterations in all presented results). Our proposed approach iteratively corrects potential misaligned ellipses using prior information.
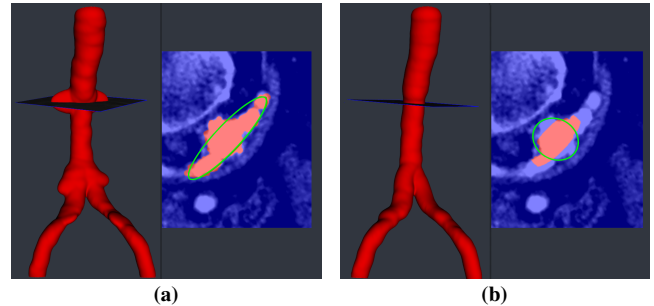


**(a)**          **(b)**

**Figure 2:** *Comparison between our approach without (a) and with (b) iterative refitting. Outliers are determined and refitted with prior knowledge of neighboring fits.*

### 3.3. Visual Mapping

After having properly fit ellipses for every edge of the vessel graph, we render the entire vessel graph. We achieve this by voxelizing the graph assuming an ellipsoid at every sampling point along the edges. The third dimension extends a specific distance ($1.5\times$ the sampling distance) to ensure a smooth transition between consecutive cross-sections. This ensures that the voxelized representation of the blood vessels is closed and connected. The larger the distance between two points, the larger the height of the ellipsoids has to be in order to avoid perceiving them in the final result. We then loop through all voxels of the data set and mark the voxels inside any ellipsoid as foreground. The resulting surface mesh is extracted using marching cubes followed by surface smoothing to remove staircase artifacts [TZG96].

The major and minor diameters of consecutive ellipses are connected with splines. This results in four bands that are colored differently: the major bands in green and the minor ones in yellow. Bifurcations have to be handled with special care, since cross-sections and their corresponding ellipses tend to intersect each other. Therefore, we connect the diameter endpoints that are closest to each other, except for the first $m$ ellipses next to the branching, where $m$ is user-defined and depends on the distance between the cross-sections. Our approach visually conveys the torsion overlaid onto the surface of the vessel itself (see Figure 1).

## 4. Results and Discussion

In this section, we present several vessel graphs showing their torsion using our elliptical cross-sectional fitting approach.

Investigations on a synthetic data set (see Figure 3) show that our approach is able to create exact fits (see Figure 3a), depicts the torsion (see Figure 3b) and establishes smooth connections between branches (see Figure 3c). In contrast, Figures 3d–3f show comparable results on a real data set. As the synthetic model is based on the skeleton of a real vessel graph, it is not perfectly smooth, since the cross-sections are not necessarily perpendicular or collinear. Our approach is based on image data instead of heuristic models, but a perfect fit to the underlying ground truth is often not possible, since these data are always noisy. Additionally, the segmentation mask is usually not accurate and contains outliers of neighboring tissue.

Figure 4 shows the robustness against outliers and noise in the input data mask. Figures 4a–4c display the original input data, whereas Figures 4d–4f present the respective ellipse fits on the processed data. Small extensions to surrounding tissue (see Figure 4a) are removed by morphological opening and closing. Outliers farther away from the center (see top-right corner of Figure 4a) are handled by the connected component analysis. Both steps are carried out during the preprocessing. Input data containing more surrounding tissue require additional steps. This especially occurs at the renal arteries where the surrounding tissue appears very similar (see Figure 4b), or at bifurcations such as the iliac arteries (Figure 4c) where the cross-sections cut into the neighboring vessel due to its tangent vector. Therefore, the peeling step iteratively crops the mask to the maximum allowed size by the neighborhood information (see Figure 4e and Figure 4f). As shown in Figure 4e and Figure 4f, the ellipses are not always perfectly fit to the processed input data, but
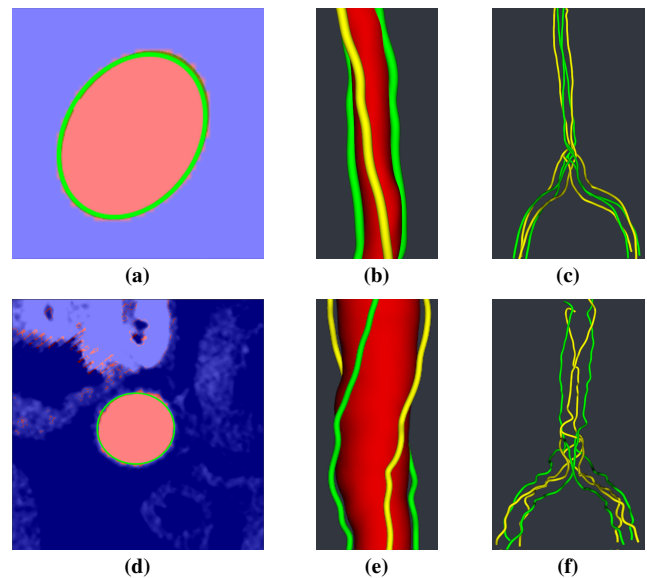


**Figure 3:** *Comparison between a synthetic (top row) and a real (bottom row) data set. (a) Ellipse fit on a cross-section. (b) Torsion of the surface (red) depicted with overlaid major (green) and minor (yellow) axis bands. (c) Torsion of the entire data set shown only with bands. (d) Ellipse fit on a cross-section. (e) Torsion on the surface (red) depicted with overlaid major (green) and minor (yellow) axis bands. (f) Torsion of the entire data set shown only with bands.*
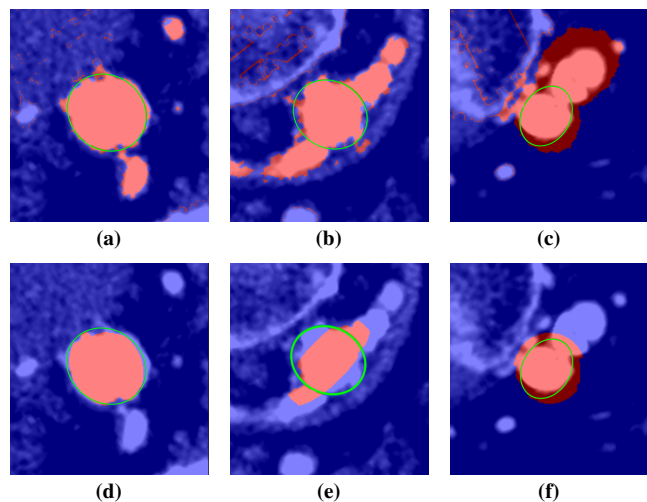


**Figure 4:** *Several cross-sections with original (top) and processed (bottom) input data. The ellipses are always based on the processed data. (a),(d) Small extensions of surrounding tissue as well as far outliers are eliminated. (b),(e) Similar surrounding tissue is reduced, insufficient fits are adapted by refitting. (c),(f) Neighboring tissue at bifurcations is eliminated by peeling.*

are reasonably good enough. This is an effect of the neighborhood information that we consider in the iterative refitting step, where outliers are rejected, refit with prior information or, ultimately, just interpolated by their neighbors.

A comparison between the fitting on the original input data and the processed data is presented in Figure 2. The aforementioned problems at bifurcations, the renal arteries or iliac arteries in our example, are handled well, but especially at the bifurcation they are still present. The main problem when visualizing torsion are sharp edges that may vanish inside the rendered vessel. Since we fit splines through the major and minor axes, sharp edges may occur. We can minimize this problem by using fewer cross-sections, i.e., larger distances between consecutive ones. This still does not remedy the problem at bifurcations, where splines between two vessels have to be connected. At this point we need to interpolate between two cross-sections, hence, the spline no longer relies on the data and may intersect the vessel, as depicted in Figure 1. Since this data set is cropped at the beginning and the mask is not well segmented, the skeleton tends to flip its tangents, which possibly results in pseudo-torsion. Even though there are slight differences in the rotation between adjacent cross-sections, torsion is a long-term process and still visible regardless of these effects. To this end, the visualization of the blood vessel itself is still reliable. Although our approach is able to limit the segmentation mask to the correct region of the vessel (see Figure 4f), a potential pseudo-torsion may occur, caused by the very coarse and inaccurate segmentation mask.

## 5. Conclusion and Future Work

In this work we presented a novel approach to compute vascular torsion that is robust against outliers. We showed that peeling and refitting are essential steps to avoid problems caused by inaccurate input data masks. We were able to create reliable surfaces out of the ellipse fits and to show the torsion on them. While our algorithm is occasionally inaccurate in single cross-sections, the torsion remains visible. The surface itself is independent from the torsion and therefore independent from rotational fitting errors. Bifurcations still pose a problem, as the bands that visually convey the torsion intersect with the vessel surface. The reason for this is that these bands are based on splines and there is no data between the branching points to avoid intersections of the cross-sections. Furthermore, our approach is data-driven, so the outcome depends on the segmentation, even if it is robust against noise and local outliers. Future work could target the problem of inaccurate input data by performing a region growing with the centerline as seed point and the corresponding ellipse as boundary. Additionally, the centerline could be recomputed by using the center of the ellipse fits, since they are robust against noise.

## References

[Ahn04]  AHN S. J.: Least squares orthogonal distance fitting of curves and surfaces in space. In *Lecture Notes in Computer Science*, vol. 3151. Springer, Berlin, Heidelberg, 2004. 3

[BMLS01]  BROWN J., MONTGOMERY K., LATOMBE J.-C., STEPHANIDES M.: A microsurgery simulation system. In *Proc. Medical Image Computing and Computer-Assisted Intervention (MICCAI)* (2001), pp. 137–144. 1

[FCCH17]  FENG Z.-G., CORTINA M., CHESNUTT J. K. W., HAN H.-C.: Numerical simulation of thrombotic occlusion in tortuous arterioles. *J Cardiol Cardiovasc Med 2*, 1 (2017), 95–111. 1, 2

[FPF99]  FITZGIBBON A., PILU M., FISHER R. B.: Direct least square fitting of ellipses. *IEEE Transactions on Pattern Analysis and Machine Intelligence 21*, 5 (1999), 476–480. 3

[GIK*10]  GEORGAKARAKOS E., IOANNOU C., KAMARIANAKIS Y., PAPAHARILAOU Y., KOSTAS T., MANOUSAKI E., KATSAMOURIS A.: The role of geometric parameters in the prediction of abdominal aortic aneurysm wall stress. *Eur J Vasc Endovasc Surg 39*, 1 (2010), 42–48. 2

[GSF*17]  GARCIA J., SANYAL A., FATEMIFAR F., MOTTAHEDI S., HAN H.-C.: Twist buckling of veins under torsional loading. *Journal of Biomechanics 58* (2017), 123–130. 1

[Han12]  HAN H.-C.: Twisted blood vessels: Symptoms, etiology and biomechanical mechanisms. *J Vasc Res 49*, 3 (2012), 185–97. 1

[HF98]  HALIR R., FLUSSER J.: Numerically stable direct least squares fitting of ellipses. In *Proc. of International Conference in Central Europe on Computer Graphics and Visualization (WSCG)* (1998), pp. 125–132. 3

[HLJ16]  HAN H.-C., LIU Q., JIANG Z.-L.: Mechanical behavior and wall remodeling of blood vessels under axial twist. *Journal of Medical Biomechanics 31*, 4 (2016), 319–326. 1

[HPSP01]  HAHN H. K., PREIM B., SELLE D., PEITGEN H.-O.: Visualization and interaction techniques for the exploration of vascular structures. In *Proc. of IEEE Visualization* (2001), pp. 395–402. 1, 2

[JKYK*16]  JOON KIM B., YANG E., KIM N.-Y., KIM M.-J., KANG D.-W., KWON S., KIM J.: Vascular tortuosity may be associated with cervical artery dissection. *Stroke 47*, 10 (2016), 2548–2552. 2

[KBT*12]  KRETSCHMER J., BECK T., TIETJEN C., PREIM B., STAMMINGER M.: Reliable adaptive modelling of vascular structures with non-circular cross-sections. *Computer Graphics Forum 31*, 3 (2012), 1055–1064. 2

[KSK16]  KANATANI K., SUGAYA Y., KANAZAWA Y.: *Guide to 3D Vision Computation*. Springer, 2016. 3

[LLC09]  LI H., LEOW W. K., CHIU I.-S.: Modeling torsion of blood vessels in surgical simulation and planning. In *Studies in health technology and informatics* (2009), vol. 142, pp. 153–158. 1, 2

[MY01]  MORI D., YAMAGUCHI T.: Construction of the CFD model of the aortic arch based on MR images and simulation of the blood flow. In *Proc. Medical Imaging and Augmented Reality* (2001), pp. 111–116. 1, 2

[OP04]  OELTZE S., PREIM B.: Visualization of anatomic tree structures with convolution surfaces. In *Proc. of IEEE/Eurographics Symposium on Visualization (EuroVis)* (2004), pp. 311–320. 1

[PO08]  PREIM B., OELTZE S.: 3D visualization of vasculature: An overview. In *Visualization in Medicine and Life Sciences* (2008), Linsen L., Hagen H., Hamann B., (Eds.), Springer, Berlin, Heidelberg, pp. 39–59. 2

[SOB*07]  SCHUMANN C., OELTZE S., BADE R., PREIM B., PEITGEN H. O.: Model-free surface visualization of vascular trees. In *Eurographics/ IEEE-VGTC Symposium on Visualization* (2007), pp. 283–290. 2

[SPSP02]  SELLE D., PREIM B., SCHENK A., PEITGEN H.-O.: Analysis of vasculature for liver surgical planning. *IEEE Transactions on Medical Imaging 21*, 11 (2002), 1344–1357. 2

[Tau91]  TAUBIN G.: Estimation of planar curves, surfaces, and nonplanar space curves defined by implicit equations with applications to edge and range image segmentation. *IEEE Transactions on Pattern Analysis and Machine Intelligence 13*, 11 (1991), 1115–1138. 3

[TBIC03]  TOPALAN M., BILGIN S. S., IP W., CHOW S.: Effect of torsion on microarterial anastomosis patency. *Microsurgery 23*, 1 (2003), 56–59. 1

[TZG96]  TAUBIN G., ZHANG T., GOLUB G.: Optimal surface smoothing as filter design. In *Proc. of the European Conference on Computer Vision* (1996), pp. 283–292. 4

[WJZL08]  WANG W., JÜTTLER B., ZHENG D., LIU Y.: Computation of rotation minimizing frames. *ACM Trans Graph 27*, 1 (2008), 2:1–2:18. 2

[WWL*10]  WU J., WEI M., LI Y., MA X., JIA F., HU Q.: Scale-adaptive surface modeling of vascular structures. *BioMedical Engineering OnLine 9*, 1 (2010), 1–16. 1, 2

[XYZ13]  XIE X., YUANYUAN W., ZHOU H.: Impact of coronary tortuosity on the coronary blood flow: A 3d computational study. *Journal of Biomechanics 46*, 11 (2013), 1833–1843. 1, 2